



Obrabotka metallov - Metal Working and Material Science

Journal homepage: http://journals.nstu.ru/obrabotka_metallov



Improving the efficiency of surface-thermal hardening of machine parts in conditions of combination of processing technologies, integrated on a single machine tool base

Vadim Skeebea ^{a, *}, Vladimir Ivancivsky ^b

Novosibirsk State Technical University, 20 Prospekt K. Marksa, Novosibirsk, 630073, Russian Federation

^a  <https://orcid.org/0000-0002-8242-2295>,  skeebea_vadim@mail.ru, ^b  <https://orcid.org/0000-0001-9244-225X>,  ivancivskij@corp.nstu.ru

ARTICLE INFO

Article history:

Received: 14 May 2021
 Revised: 14 June 2021
 Accepted: 07 August 2021
 Available online: 15 September 2021

Keywords:

Hybrid equipment
 High energy heating
 Machining
 Induction hardening
 Conceptual design

Funding

The research was funded by RFBR and Novosibirsk region, project number 20-48-540016.

Acknowledgements

Research were conducted at core facility “Structure, mechanical and physical properties of materials”.

ABSTRACT

Introduction. In the manufacturing industry, there is a particular interest in the development of a new type of technological equipment, which makes it possible to implement methods for modifying the parts surface layers by processing it with concentrated energy sources. The combination of two processing technologies (mechanical and surface-thermal operations) in the conditions of integrated equipment makes it possible to neutralize the disadvantages of monotecnologies and obtain new effects that are unattainable when using technologies separately. The use of hybrid machine tools in conjunction with the developed technological recommendations will allow achieving a multiple increase in the technical and economic efficiency of production, resource and energy saving, which in turn will contribute to an increase in the competitiveness of products and the renewal of the technological paradigm. **Purpose of work:** increasing productivity and reducing energy consumption during surface-thermal hardening of machine parts by exposure to concentrated energy sources under conditions of integrated processing. **Theory and methods:** studies of the possible structural composition and layout of hybrid equipment during the integration of mechanical and surface-thermal processes are carried out taking into account the main provisions of structural synthesis and the components of metalworking systems. Theoretical studies are carried out using the basic provisions of system analysis, geometric theory of surface formation, design of metalworking machines, finite-element method, mathematical and computer simulation. Mathematical simulation of thermal fields and structural-phase transformations in the case of HEH HFC is carried out in the ANSYS and SYSWELD software packages, using numerical methods for solving the differential equations of unsteady thermal conductivity (Fourier's equation), carbon diffusion (Fick's second law), and elastoplastic behavior of the material. The verification of the simulation results is carried out by conducting field experiments using: optical and scanning microscopy; mechanical and X-ray methods for determining residual stresses. In the study, Uone JD520 and Form Talysurf Series 2 profilograph-profilometers are used to simultaneously measure shape deviations, waviness and surface roughness. Surface topography is assessed using a Zygo New View 7300 laser profilograph-profilometer. The microhardness of the hardened surface layer of parts is evaluated on a Wolpert Group 402MVD device. **Results and discussion.** An original method of structural-kinematic analysis for pre-design research of hybrid metalworking equipment is presented. Methodological recommendations are developed for the modernization of metal-cutting machine tools, the implementation of which will allow the implementation of high-energy heating by high-frequency currents (HEH HFC) on a standard machine-tool system and ensure the formation of high-tech technological equipment with expanded functionality. A unified integral parameter of the temperature-time effect on a structural material is proposed when the modes of hardening by concentrated heating sources are assigned, which guarantee the required set of quality indicators of the surface layer of machine parts, while ensuring energy efficiency and processing productivity in general. It is experimentally confirmed that the introduction into production of the proposed hybrid machine tool in conjunction with the developed recommendations for the purpose of the HEH HFC modes in the conditions of integral processing of a “Plunger bushing” type part in relation to the factory technology allows increasing the productivity of surface hardening by 3.5...4.1 times, and reduce energy consumption by 9.5...11.3 times.

For citation: Skeebea V.Yu., Ivancivsky V.V. Improving the efficiency of surface-thermal hardening of machine parts in conditions of combination of processing technologies, integrated on a single machine tool base. *Obrabotka metallov (tekhnologiya, oborudovanie, instrumenty) = Metal Working and Material Science*, 2021, vol. 23, no. 3, pp. 45–71. DOI: 10.17212/1994-6309-2021-23.3-45-71. (In Russian).

* Corresponding author

Skeebea Vadim Yu., Ph.D. (Engineering), Associate Professor
 Novosibirsk State Technical University,
 20 Prospekt K. Marksa,
 Novosibirsk, 630073, Russian Federation
 Tel: 8 (383) 346-17-79, e-mail: skeebea_vadim@mail.ru

Introduction

In the era of globalization and high competitiveness, it is extremely important for modern mechanical engineering to work on reducing production costs and at the same time ensuring the production of high-quality products with maximum productivity [1-20]. In this regard, the manufacturing industry clearly shows a particular interest in the development of a new type of technological equipment that allows implementing methods for modifying the surface layers of parts by processing it with concentrated energy sources [21-25]. Local and ultra-high-speed thermal effects make it possible to obtain higher values of hardness, strength, and toughness due to the formation of a highly dispersed metastable structure on the surface of the parts with a much higher dislocation density compared to bulk processing and traditional methods of surface hardening [17, 21–23, 26–31].

The development of high-frequency heating technology associated with the use of radio frequencies, with the work on the miniaturization of inductors and equipping it with ferrite magnetic cores, led to the emergence of a new method – high-energy heating with high-frequency currents (HEH HFC), which is currently of particular interest from the point of view of strengthening structural steels [26-28, 32-36]. This method makes it possible to implement the technological process of quenching with specific heating capacities of about 400 MW/m^2 , which successfully allows it to compete with other concentrated sources (laser, electron beam) when hardening the material without melting (Fig. 1). It should be noted that the provision of the required constant gap ($\delta = 0.1 \dots 0.2 \text{ mm}$) between the inductor and the workpiece, which is a necessary condition for the implementation of the HEH HFC, becomes possible only when combining two processing technologies – mechanical and surface-thermal operations – on a single machine base [20, 27, 28, 37]. Since the development of new machine tools requires a large amount of financial and labor resources, we propose the modernization of standard metal-cutting machines by retrofitting it with an additional concentrated energy source, which can be used as a HFC generator. Taking into account the current level of development of microprocessor technology in the field of high-frequency industrial thyristor-type installations, as well as the criteria for digestible integration into a standard machine system, our area of interest will include high-frequency generators of the microwave type. At the same time, it becomes an urgent task to develop new methods for assigning processing modes that consider the combined operations of the technological process not in isolation, but in interrelation, and allow obtaining parts with a predetermined accuracy and physical and mechanical properties of its working surfaces [27, 28].

The phase transformations, and, consequently, the resulting structure and quenching depth, as well as the grain size of austenite depend on the integral temperature-time effect of heating on the steel structure and, therefore, are also determined by the shape of the thermal curve. The use of the average rate of heating and maximum heating temperature as the main parameters for the purpose of surface quenching modes is rather approximately characterized by the temperature-time conditions of phase transformations during austenitization of steel [28, 38-40]. In addition to the above parameters, it is necessary to take into account both the average cooling rate and residence time of the material in the temperature range of phase trans-

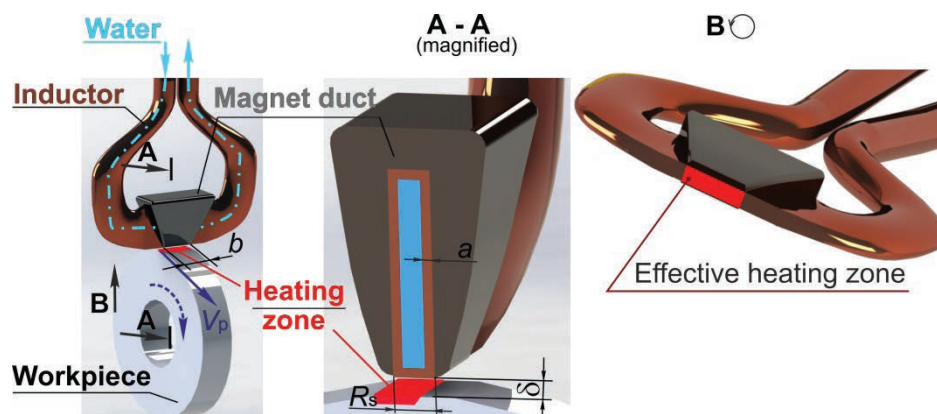


Fig. 1. The scheme of HEH HFC processing

formations. Therefore, the processing modes should be assigned in such a way as to provide the necessary thermal cycles with the specified parameters in the surface layers of the material [27, 28]. At the same time, as it was shown in studies [27, 41], it is not possible to establish an unambiguous relationship of the numerical values of these parameters with the processing modes and quality characteristics of the hardened layer. However, it is obvious that the numerical values of the parameters of thermal cycles are determined by the magnitude of the transmitted energy and the nature of its distribution in the material.

In this regard, and on the basis of the works [41, 42], it is proposed to use the integral temperature-time characteristic S , which combines all the listed parameters of thermal cycles [28, 43–45], as the main parameter of the purpose of surface hardening modes. The process of austenite formation will occur in the time period $\tau_t = \tau_3 - \tau_1$ (Fig. 2) regardless of whether the thermal curve has an upward or downward character in a given time period. This means that the total time τ_t and the temperatures at which the austenitization process occurs can be characterized by the area value (S_{ABC}) limited at the top by the heating curve, and at the bottom – by a straight line corresponding to the temperature A_{C1} .

$$S = \int_{\tau_1}^{\tau_3} T(\tau) d\tau - A_{C1}(\tau_3 - \tau_1), \quad (1)$$

The physical meaning of this characteristic becomes clear from the dependence

$$S = Q \cdot R_T$$

where Q is the energy, J; R_T is the thermal resistance of the material, °C s/J.

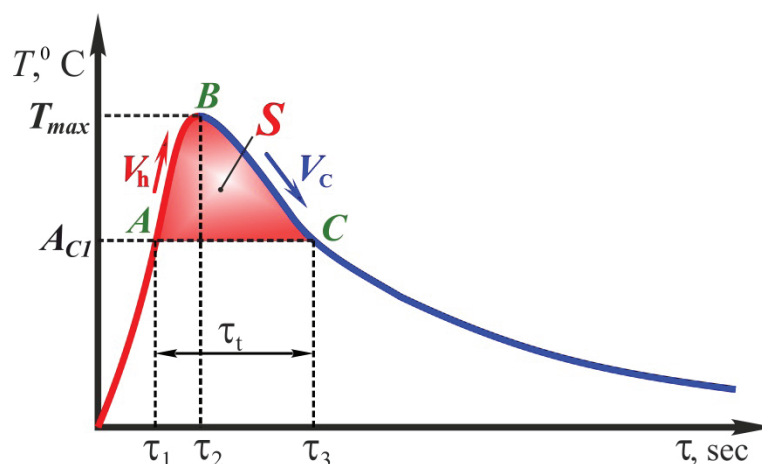


Fig. 2. Kinetic curve of steel heating and cooling during quenching

The thermal resistance of a metal is the ability of a material to resist heat transfer. In this case, we consider a metal heated above the temperature A_{C1} . In this case, the numerical value of the thermal resistance of the metal will depend not only on the thermal conductivity coefficient, but also on the structural-phase transitions that mainly occur in this temperature range endothermically with heat absorption. In other words, this characteristic indirectly determines the amount of energy transferred to the material and spent on structural-phase transformations. It can be easily calculated from the dependence (1) in the process of simulation temperature fields in the material [28].

Based on the above, in order to develop a methodology for assigning surface hardening modes in hybrid processing conditions, it is necessary to establish the relationship of the numerical values of the integrated temperature-time characteristic with the processing modes, on the one hand, and with the hardening depth, on the other hand. The solution of this problem is carried out by combined simulation of temperature fields and structural-phase transformations in the material [27, 28, 39, 44, 45].

Due to the fact that the issues of developing new hybrid machine tool systems belong to critical production and industrial technologies, there is a lack of experimental work in the literature aimed at analyzing the effectiveness of its design and implementation.

Purpose of work is to increase productivity and reduce energy consumption during surface-thermal hardening of machine parts by exposure to concentrated energy sources under conditions of integrated processing.

To achieve this purpose, it is necessary to solve the following tasks:

1. To propose a method of structural analysis that makes it possible to perform effectively pre-design studies in the development of hybrid metalworking equipment and to prove the possibility of embedding a concentrated energy source in a standard machine system.

2. To establish the relationship of the numerical values of the operating parameters of the HEH HFC on the quality characteristics of the surface layer of the processed parts. To develop a methodology for assigning high-energy heating modes with high-frequency currents in integrated processing conditions.

3. To test industrially a complex of equipment that implements the HEH HFC technology, proving the effectiveness of its introduction into production.

Experimental technique

To determine the executive movements of a hybrid metalworking system (HMS) and the required number of its configurable parameters, the main provisions of the structural and kinematic synthesis of metal-cutting machines were used [37, 46, 47]. Studies of the possible structural composition and layout of HMS during the integration of mechanical and surface-thermal processes were carried out taking into account the main provisions of structural synthesis and the components of metalworking systems presented in [37, 48–56].

To solve the problem of determining the operational loads of a hybrid metalworking system, a universal method was used to substantiate the technical characteristics of integrated machine equipment based on mathematical simulation of its operating conditions [57, 58].

Materials and methods of field experiments

A plunger barrels (Fig. 3) made of *steel 45* and *U8A* were selected as samples for field experiments (Table 1). The composition of the starting material was determined using an *ARL 3460* optical emission spectrometer.

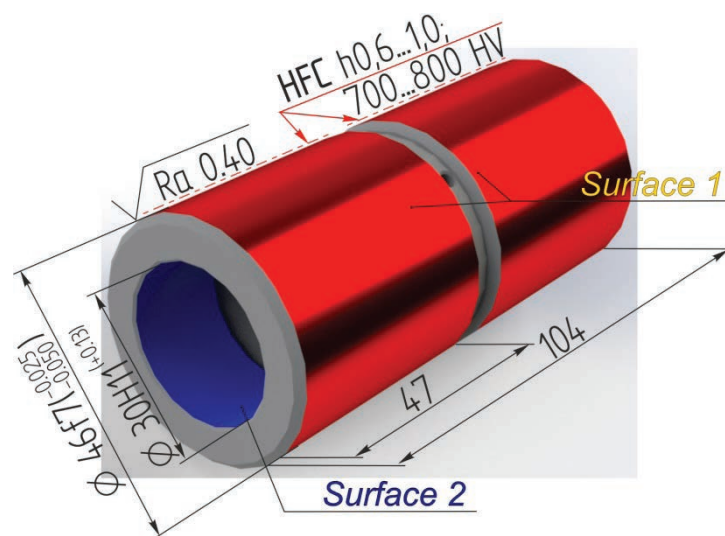


Fig. 3. Plunger barrel

Chemical compositions of initial material

Steel grade	Weight of elements, [%]							
	<i>C</i>	<i>Si</i>	<i>Mn</i>	<i>S</i>	<i>P</i>	<i>Cr</i>	<i>Ni</i>	<i>Cu</i>
45	0.44	0.23	0.61	0.013	0.019	0.11	0.15	0.17
U8A	0.80	0.21	0.21	0.017	0.022	0.11	0.15	0.18

The final stage of the factory technological process of manufacturing the part consisted of the following operations: turning (turning and screw-cutting lathe model 16K20); hardening of HFC (industrial tube generator brand *VCHG 6-60/0.44* with an operating current frequency of 440 kHz); grinding (circular grinding machine model *3M151V*). The finishing mechanical operation is carried out according to the mortise grinding scheme. At the same time, the processing cycle is divided into three stages: preliminary grinding, final grinding and sparkout. Due to the fact that the processing is carried out on a hardened surface and in order to avoid changing the properties of the surface layer, grinding is carried out on “soft” modes. Pre-grinding is carried out in the following modes: the value of the excess material $t = 0.2$ mm, the workpiece speed $V_p = 30$ m/min, the radial feed $S_r = 0.004$ mm/rev. Final grinding – $t = 0.1$ mm, $V_p = 30$ m/min, $S_r = 0.001$ mm/rev. The time of sparkout is $\tau_s = 10$ s.

The final stage of the technological process of manufacturing a part using hybrid metalworking equipment was carried out on a modernized screw-cutting lathe of the *UT16PM* model and consisted of three transitions: turning, surface hardening using the HEH HFC, diamond smoothing. The machine system was equipped with an additional energy source, which was used as an ultra-high-frequency generator of the microwave-10 thyristor type with an operating current frequency of $440 \times \text{kHz}$. A digital oscilloscope of the *Hantek DSO 1000S Series* model was used to measure and control the operating frequency of the induction heater.

Rough turning was carried out with a pass-through cutter equipped with replaceable polyhedral plates (RPP) (cutting plate material is a hard alloy of the following composition: WC 79 %, TiC 15 %, Co 6 %), in the following modes: $V_p = 90$ m·min⁻¹; $S_o = 0.35$ mm/rev.; $t = 1$ mm. During surface quenching, a loop-type inductor equipped with ferrite of the *N87* grade was used. The heating process was carried out according to a deep scheme (the thickness of the hardened layer did not exceed the depth of current penetration into the hot metal – 0.6...0.8 mm) in a continuous-sequential way [14, 15, 24, 26]. The studies were carried out using intensive water shower cooling of the surface in the following range of processing modes: the specific power of the source $q_s = (1.5-4.0) \times 10^8$ W m⁻², the speed of movement of the part under the inductor $V_p = (0.05...0.1)$ m s⁻¹. The width of the active inductor wire was $R_s = 2$ mm, and its length $b = 10$ mm. The processing was carried out with a gap of $\delta = 0.1...0.2$ mm. Finishing turning was performed in the following modes: $V_p = 130$ m/min ($n_p = 882$ min⁻¹); $S_o = 0.025$ mm/rev.; $t = 0.01...0.015$ mm. For rough and finish turning, the sulfurized mineral oil “Sulfofresol” was used as a coolant-cutting fluid (CCF). Diamond smoothing was carried out according to a two-pass scheme using a designed and manufactured holder with an elastic head, in which diamond tips (TU2-037-631-88) of radius $R = 1$ mm were installed. The radial component of the smoothing force of the P_y , taking into account the rigidity of the technological equipment, the hardness of the surface layer of the workpiece after surface hardening of the HFC (700...800 HV) and the radius of the diamond sphere, respectively, was equal to 150 N. At the same time, the circumferential speed of the workpiece was $V_{smooth} = 24$ m/min; and the feed values were $S_{O\ smooth} = 0.018$ mm/rev. Industrial oil of the I-20A brand was used as a coolant-cutting fluid for diamond smoothing [59].

To determine the linear operational dimensions, the theory of dimensional chains and the method presented in [60, 61] were chosen according to the conditions of ensuring the required depth of the heat-strengthened layer.

In the study, the *Uone JD520* and *Form Talysurf Series 2* profilograph profilometers were used to simultaneously measure shape deviations, waviness and surface roughness. The surface topography was evaluated using a *Zygo New View 7300* laser profilograph profilometer.

Structural studies of the samples were carried out using a *Carl Zeiss Axio Observer Z1m* optical microscope and a *Carl Zeiss EVO 50 XVP* scanning electron microscope equipped with an *INCA X-ACT* energy dispersion analyzer (Oxford Instruments). The microstructure of the samples was detected by etching with a 5-% alcohol solution of nitric acid, as well as a saturated solution of picric acid in ethyl alcohol with the addition of surfactants [62].

The microhardness of the hardened surface layer of the parts was evaluated using the *Wolpert Group 402MVD* device. Studies of residual stresses were carried out using the X-ray method on a high-resolution diffractometer *ARL X'TRA* and a mechanical destructive method – layer-by-layer electrolytic etching of the sample [63, 64]. To identify defects in the surface layer at each transition, the following methods were used: optical method using a *Carl Zeiss Axio Observer A1m* microscope, capillary method, eddy current method using an eddy current flaw detector *VD-70*.

Statistical processing of the results of experimental studies was performed in the software products *Statistica*, *Table Curve 2D* and *Table Curve 3D*.

Mathematical simulation of thermal fields and structural-phase transformations in the HEH HFC

The finite element model was constructed in the software complexes *ANSYS* and *SYSWELD*, which use numerical methods for solving differential equations of non-stationary thermal conductivity (Fourier equation), carbon diffusion (Fick's 2nd law) and elastic-plastic behavior of the material [27, 28, 33, 34, 38–40, 43–45].

The preparation of the finite element model was carried out in the *ANSYS* software package. The *ANSYS Meshing* generator formed a hexahedral finite element grid using the following types of finite elements: *Solid bodies* – solid bodies were modeled with 8-node *SOLID 45* tetrahedra; *Surface bodies* – surface bodies were modeled with 4-node 4-angle shell elements – *SHELL 63*; *Line bodies* – line bodies were modeled with 2-node *LINK 8* linear elements. The size of the finite elements was 0.01...1 mm. When creating a finite element model, the following components were created: “*Volume*” – a group of three-dimensional elements denoting the object being processed; “*Trajectory*” – a group of one-dimensional elements that determines the trajectory of a high-concentration energy source; “*Reference*” – a reference equidistant – a group of one-dimensional elements that helps orient the local coordinate system of the energy source; “*StartElem*” – starting elements of the beginning of the source action; “*StartNodes*” and “*EndNodes*” – the initial and final nodes on the trajectory of movement; “*Skin*” is a group of two-dimensional elements denoting the surfaces on which convective and radiative heat losses occur; “*ClampedNodes*” is a group of nodes on which the disk is fixed (Fig. 4).

Simulation of the process of high-energy heating by high-frequency currents was carried out in the *SYSWELD* software package, which allows using a model of elastic-viscoplastic behavior of the material and modern mathematical apparatus to calculate temperature fields, the distribution of structural components, internal stresses and deformations. During the preparation of the finite element model, the specifics of the distribution of the specific power of the HFC heating source directly under the inductor and along the depth of the material were taken into account [27, 28, 33, 34, 38–40, 43–45].

Results and its discussion

When developing integrated metalworking equipment, it is planned to implement a method of high-energy heating with high-frequency currents at one of the technological transitions of a hybrid machine. Taking into account the design features of inductors for HEH HFC, the formation of the production lines of the treated surface occurs by localized heating areas, the dimensions of which are determined by the width of the active inductor wire and the length of the ferrite magnetic core (Fig. 1). As a result, to ensure surface quenching, exactly the same coordinated relative movements of the workpiece and the tool are required as when forming through the processes of turning and diamond smoothing (Fig. 5). Structural and kinematic

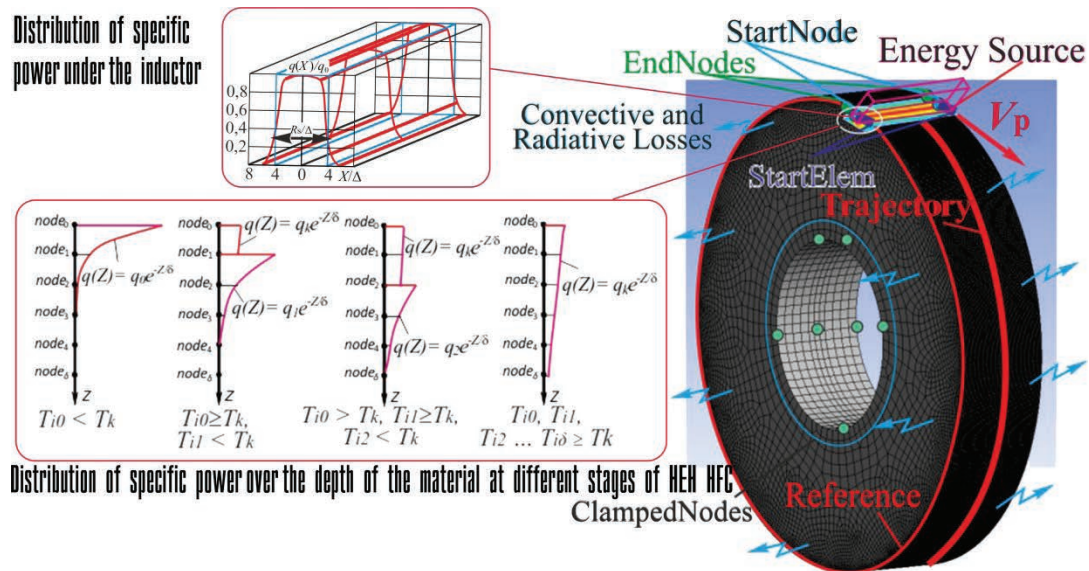


Fig. 4. Finite element model of the HEH HFC process

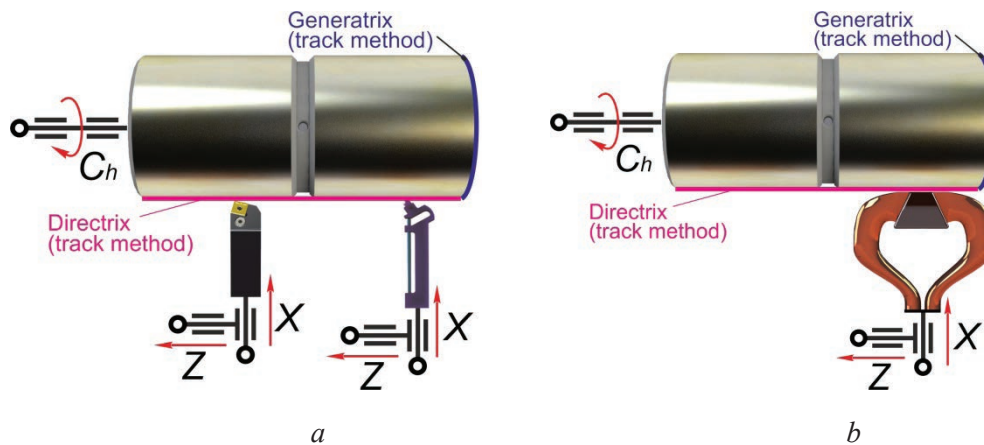


Fig. 5. Generation of geometry (cylindrical surface):

a – during machining (turning and diamond smoothing); b – during surface hardening by HEH HFC with loop inductor with a magnetic core

analysis showed the complete identity of the necessary set of executive movements and the complex of parameters configured in it at all transitions (turning, HEH HFC hardening and diamond smoothing) of integrated processing.

Figure 6 shows the partial structural formulas of the layouts in combination with structural-kinematic schemes (SKS) for each processing method separately. The subsequent synthesis of the generalized kinematic structure of the hybrid metalworking system under development was carried out according to the scheme of aggregate modular layout configuration. With this method, the layout formula can be represented as follows: $C_n 0Z(Xrd_1+WUd_2)$ (Fig. 7).

Based on the combined analysis of the required structural formula for the layout of hybrid equipment, the kinematic structure of the *UT16PM* machine and the rigidity of its base units, the main directions of modernization of this model of metalworking equipment were identified. The conducted complex of pre-project studies allowed us to prepare working documentation for the implementation of hybrid technological equipment combining mechanical and surface-heat treatment (Fig. 8).

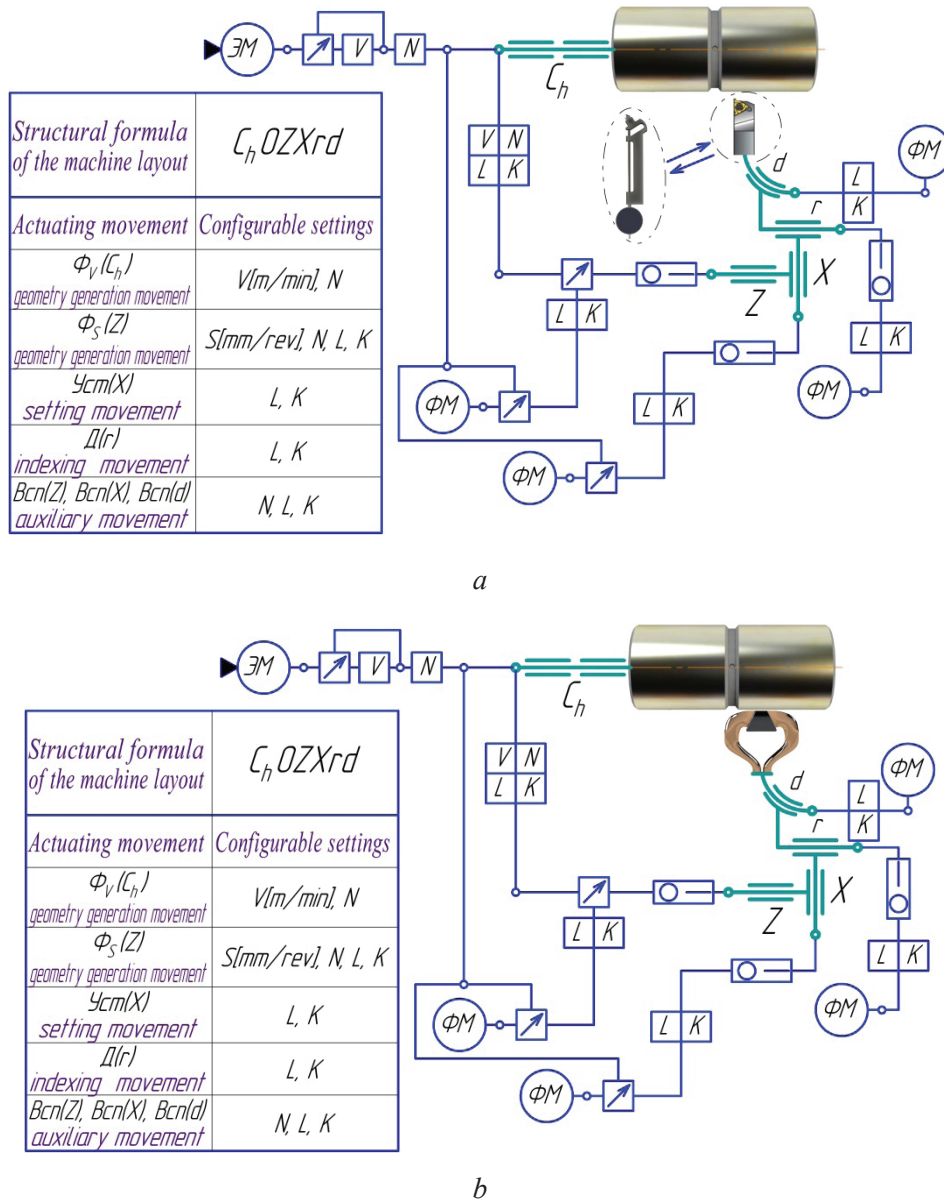


Fig. 6. Structural kinematic schemes for processing a cylindrical surface:

a – turning and diamond smoothing; *b* – surface hardening by HEH HFC with loop inductor with a magnetic core

Simulation of the technical characteristics of hybrid metalworking equipment has shown that in order to ensure a level of forming performance comparable to mechanical operations, it is necessary to process HEH HFC at speeds of the order of $V_p \in [50, 100]$ mm/s. Conducting field experiments allowed us to determine the range of specific power of the source $q_s(h, V_p)$, with which it is required to process the HEH HFC: $q_s \in [1.5; 4.0] 10^8$ W/m². To ensure the lower frequency range of the spindle with the workpiece rotation, the main motion drive was upgraded, consisting in its retrofitting with a frequency converter *HF Inverter model F1500-G0015S2B*.

Confirmation of the effectiveness of the implementation of the developed hybrid equipment is considered using the example of the finishing stage of the technological process of plunger barrel processing (Fig. 3), built according to two different schemes: according to the factory technology and using the proposed integrated processing.

The final stage of the existing technological process of manufacturing a plunger barrel includes the following operations: turning, HEH HFC hardening and grinding (table 2). According to the conditions of the drawing, the outer cylindrical surface 1 should have a hardened layer with a depth of 0.6...1.0 mm with a

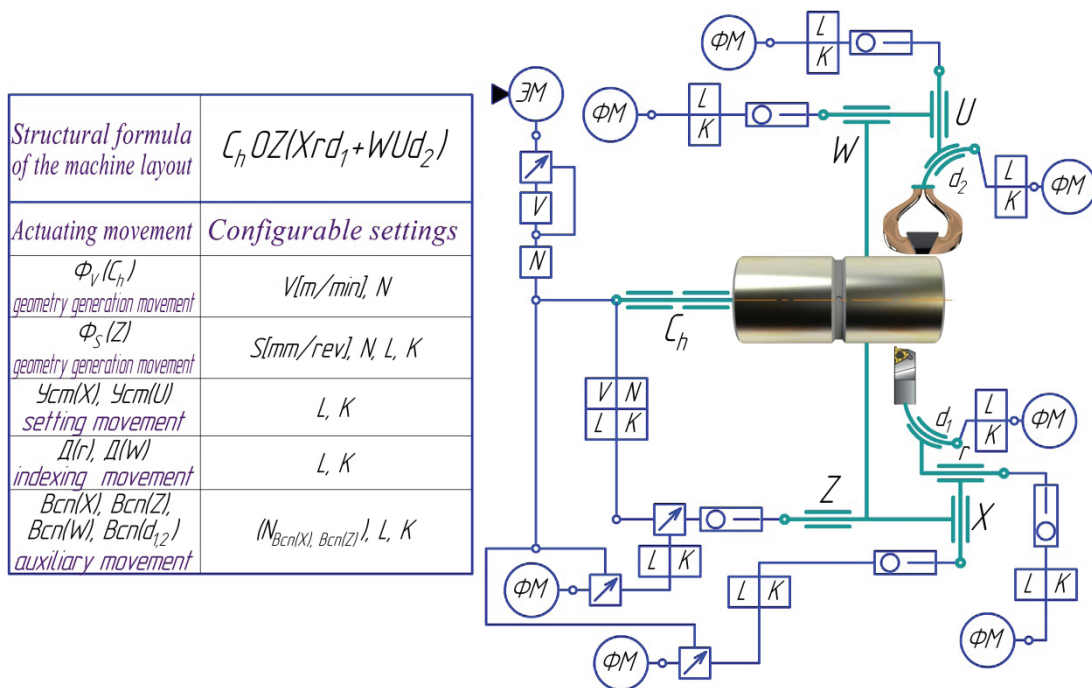


Fig. 7. Structural kinematic scheme of the hybrid metalworking system: the structural formula is $C_h OZ(Xrd_1+WUd_2)$

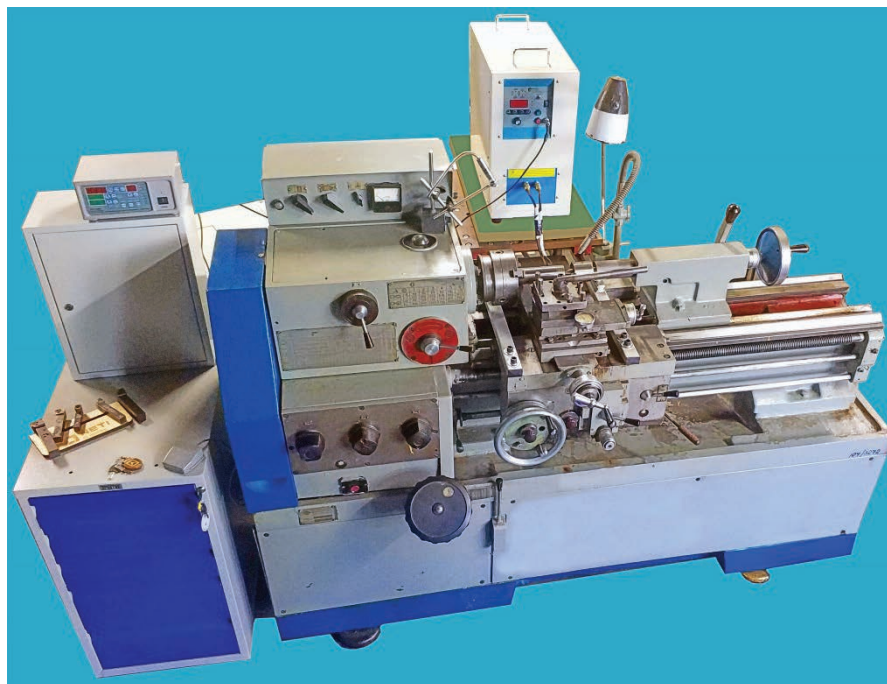


Fig. 8. Hybrid metal working machine

surface microhardness level of 700...800 HV. It is required to determine: the size D_1 , the tolerance for which is set; the technological depth of HEH HFC hardening A_T and the tolerance for it δ_T ; the minimum allowance for final processing z_{min} .

The solution of this problem was carried out according to the method presented in [61], according to which $D_1 = D_{i-1}$ and $\delta_{i-1} = 0.1 \text{ mm}$, $A_K = 0.6...1.0 = 0.6^{+0.4} \text{ mm}$, the tolerance of the closing link $\delta_K = 0.4 \text{ mm}$.

1. To determine the permissible variation of the cutting depth δ_p , it is necessary to know the value of the tolerance for the HFC hardening depth δ_T , which, as a rule, is determined on the basis of experimental data. HFC quenching is carried out with the stabilization of the supplied power. In this case, the main criterion



The initial data on the allowances and operating dimensions calculation for the processing of the hardened surface

Operation No.	Draft	The operation and technical requirements for its implementation
15		Turning the surface 1. Ellipticity within tolerance on diameter D_1 which is to be determined
20		Surface 1 hardening by HFC at the depth A_T . The hardness of the hardened surface is 700...800HV. Increase in D_1 diameter caused by the 8 ... 10 μm swelling per each millimeter of the hardened layer thickness.
25		Finish grinding of the surface 1

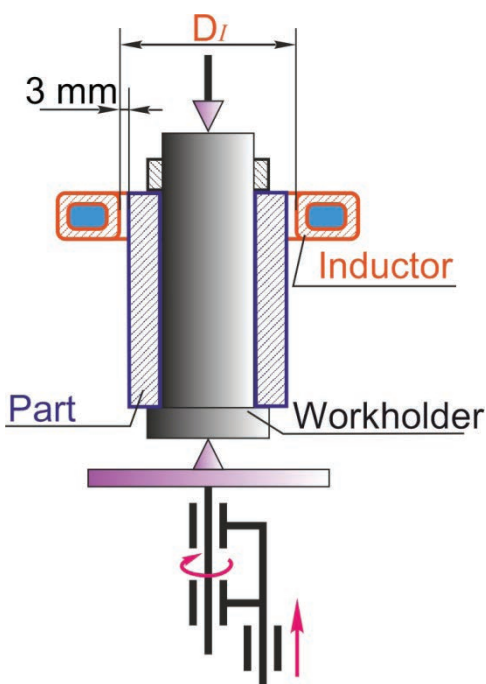


Fig. 9. Diagram of workpiece HFC hardening by the standard technology

determining the change in the depth of the hardened layer is the constancy of the gap between the inductor and the heated surface.

According to the factory technology, the part is based on the surface 2 on a rigid mandrel installed in the centers. Quenching is carried out in a continuous-sequential way using an annular inductor $D_i^{+0.74}$ ($D = 52 H14$) (Fig. 9). The technological gap between the inductor and the part is 3 mm. In this case, the change in the gap is due to the displacement of the center of rotation of the part, which is determined by the error of the shape of the inductor and the error of the part positioning.

To obtain a circumferentially symmetrical layer, the rotation of the part is used. According to experimental data, it was found that for these conditions of HFC quenching, provided that the inductor is aligned relative to the axis of the centers $-\delta_T = 0.1$ mm. In this case, we have $\delta_i = 0.4 - 0.1 = 0.3$ mm.

2. We determine the permissible value of the total spatial deviation $\sum \delta_{ei}$, taking into account the operational tolerances for misalignment δ_{ei} , the sequence of operations, the methods of basing and positioning.

According to the data of [27, 28, 65], for carbon steels, the increase in the specific volume of the quenched surface is 0.5 %. During surface quenching, when the directions of free expansion

are limited, we can expect an increase in the diameter by 8...10 μm for each millimeter of the thickness of the hardened layer. In our case, the quenching depth according to the factory technology is 1.05...1.15 mm, therefore the value of $A_p = 0.0084...0.0115$ mm, $\delta_p = 0.0031$ mm. Based on this, you can determine the value of the tolerance δ'_{i-1} .

$$\delta'_{i-1} = \delta_{i-1} + \delta_p = 0.1 + 0.0031 = 0.1031 \text{ mm}$$

$$\text{In this case } 2\delta_{e\Delta} = \delta_t - \frac{\delta_i + \delta'_{i-1}}{2} = 0.3 - \frac{0.025 + 0.1031}{2} = 0.23595 \text{ mm.}$$

3. Determine the possible value of the spatial deviations $\sum \delta_{ei}$, taking into account the operational tolerances δ_{ei} for misalignment, the sequence of operations, the methods of basing and positioning.

At finishing operations 20 and 25, the factory technology provides for processing on a rigid mandrel. In this case, the error of basing the part on a rigid mandrel can be determined as follows

$$\varepsilon_{B1} = \delta_0 + \delta_1 + \delta_2 = 0.02 + 0.13 + 0.021 = 0.171 \text{ mm,}$$

where δ_0 is the minimum gap, δ_1, δ_2 are the tolerances of the hole and mandrel, mm.

The error of basing the mandrel in the centers of $\varepsilon_{B2} = 0.02$ mm. The error of fixing the part and the mandrel $\varepsilon_F = 0.03$ mm. The total error of the part positioning is determined as:

$$\varepsilon_p = \varepsilon_{B1} + \varepsilon_{B2} + \varepsilon_F = 0.171 + 0.02 + 0.03 = 0.221 \text{ mm.}$$

In addition to the positioning error, the value of the total spatial deviation is influenced by the amount of deformation δ_c and (curvature, warping) of the hollow cylinder after surface hardening, which occurs due to the uneven depth of the hardened layer and depends on the wall thickness, the ratio of the wall thickness and the cylinder diameter, and the relative depth of the hardened layer. Hardening of the outer surface leads to the appearance of a "barrel". For this case, the value of $\delta_c = 0.010$ mm. Then

$$2\sum \delta_{ei} = \varepsilon_p + \delta_c = 0.221 + 0.010 = 0.231 \text{ mm}$$

In this case, the condition $\sum \delta_{ei} \leq \delta_{e\Delta}$ is being executed.

4. We determine the desired size – the technological depth of the heat-strengthened layer A_T . Limit values of the closing size

$$A_{K\max} = A_{T\max} - t_{\min} \quad \text{and} \quad A_{K\min} = A_{T\min} - t_{\max} \quad (2)$$

High-quality final surface processing after thermal hardening is possible under the condition $t_{i\min} \geq (R_z + T)_{i-1}$, where R_z, T is the surface roughness and the depth of the defective layer on the previous processing. Such a minimum value of the allowance should also be provided for an unfavorable combination of parameter values that affect its value: when $D_{i-1\max}$ and $D_{i-1\min}$. At operation 15, a semi-rough turning is carried out: $R_z = 0.05$ mm, $T_{i-1} = 0.05$ mm. Hence, $t_{\min} = 0.05 + 0.05 = 0.10$ mm, and $t_{\max} = t_{\min} + \delta_t = 0.10 + 0.30 = 0.40$ mm.

Solving equations (2) with respect to the desired size, we obtain

$$A_{T\max} = A_{K\max} + t_{\min} = 1.0 + 0.10 = 1.10 \text{ mm;}$$

$$A_{T\min} = A_{K\min} + t_{\max} = 0.6 + 0.4 = 1.0 \text{ mm.}$$

5. Determine the allowance for final processing by the equation

$$z_{i\min} = 2(R_z + T)_{i-1} + 2\sum \delta_{ei} = 2 \times 0.10 + 0.231 = 0.431 \text{ mm.}$$

6. In this case, the size of the preprocess of the surface 1, taking into account the swelling, will be equal to $D_{i-1} = D_i + z_{i\min} + \delta_{i-1} - A_{R\min}$, then $D_1 = 46 + 0.431 + 0.10 - 0.008 = 46.523$ mm. According to the factory technology, D_1 is assumed to be equal to 46.5 mm.

Thus, the desired parameters are: the technological depth of quenching $A_T = 1.0^{+0.1}$ mm; the size of the preprocess $D_l = 46.5^{-0.1}$ mm; the allowance for final processing $z_{\min} = 0.431$ mm. It should be noted that 5...8 % of the parts are rejected due to the presence of burns and microcracks on the surface (according to the company).

To ensure this depth of the hardened layer when using a generator with a frequency of 440 kHz, it is necessary to implement a surface heating scheme, which is usually characterized by lower values of the specific power and speed of movement of the heating source in relation to the volumetric scheme. With the width of the active inductor wire $R_s = 12$ mm – $q_s = 1.2 \times 10^7$ W/m², $V_p = 2$ mm/s.

Two sections with a total length of 94 mm should be hardened on the parts. Both sections are processed in one axial movement of the part relative to the annular inductor. The total length of the part motion, taking into account the presence of a groove with a width of 6 mm and the entry and exit of the inductor with a continuously sequential heating scheme, is $l = 114$ mm. In this case, the processing time is $T_p = l/V_p = 57$ s, while according to general machine-building standards for heat treatment on HFC installations with the specified method of basing the part (Fig. 9), the auxiliary time of the $T_{aux} = 20$ s. Thus, the piece productivity is equal to

$$P_p = 1 / (T_p + T_{aux}) = 1 / (57 + 20) = 0.013 \text{ s}^{-1}$$

and energy costs are equal to

$$E = (q_s \cdot \pi \cdot D_l \cdot R_s \cdot l) / V_p = (1.2 \cdot 10^7 \cdot 0.0465 \cdot 0.012 \cdot 0.114) / 0.002 \approx 0.333 \text{ kW} \cdot \text{h}$$

The final stage using the proposed integrated processing. In this case, the three finishing operations are replaced by one integrated, consisting of three transitions: 1. Turning (rough, semi-finishing, single finishing); 2. HEH HFC hardening; 3. Final finishing turning and diamond smoothing (Table 3).

1. HFC quenching is carried out according to the scheme (Fig. 10). In this case, the unevenness of the hardened layer in depth is determined by the accuracy of manufacturing the active inductor wire and its position relative to the axis of the processed product. Based on the experimental results and using the alignment of the active inductor wire according to the indicator $\delta_T = 0.05$ mm. Hence, $\delta_t = \delta_K - \delta_T = 0.4 - 0.05 = 0.395$ mm.

2. The quenching depth is 0.6...1.0 mm, hence the value of $A_p = 0.0048...0.010$ mm, $\delta_p = 0.0052$ mm. Thus,

$$\delta'_{i-1} = \delta_{i-1} + \delta_p = 0.01 + 0.0052 = 0.0152 \text{ mm.}$$

Then the permissible value of the total spatial deviation will be equal to

$$2\delta_{e\Delta} = \delta_t - \frac{\delta_i + \delta'_{i-1}}{2} = 0.395 - \frac{0.025 + 0.0152}{2} = 0.3749 \text{ mm.}$$

3. The proposed finishing stage of the technological process is carried out without repositioning the workpiece, therefore, despite the fact that the same tooling is used, the positioning error is $\varepsilon_p = 0$. The first transition – rough, semi-finishing turning of the surface allows to eliminate errors that occurred at the previous stage of the technological process and errors in the part positioning. This, in turn, ensures the constancy of the gap between the inductor and the treated surface, and, consequently, the uniformity of the depth of the hardened layer. In this case, the amount of warping after surface hardening is $\delta_{\mu} = 0$. Then $2\sum\delta_{ei} = 0$.

The real value of δ_t is

$$\delta_t = \sum\delta_{ei} + \frac{\delta_i + \delta'_{i-1}}{2} = 0 + \frac{0.025 + 0.0152}{2} = 0.0201 \text{ mm.}$$

4. The final finishing turning is carried out after quenching, therefore, $T_{i-1} = 0$. Due to the fact that surface hardening is carried out without changing the surface roughness, and mechanical processing is carried out with a single grinding wheel, the achievement of the surface roughness specified by the drawing

Initial data for the calculation of allowances and operational dimensions for the treatment of the hardened surface using integrated processing

Transition No.	Draft	The operation and technical requirements for its implementation
1		<p><i>Turning the surface 1.</i> Ellipticity within tolerance on diameter D_1 which is to be determined.</p>
2		<p><i>Surface 1 hardening by HFC</i> at the depth A_T. The hardness of the hardened surface is 700...800 HV. Increase in D_1 diameter caused by the 8 ... 10 μm swelling per each millimeter of the hardened layer thickness.</p>
3		<p>Final finish turning and diamond smoothing of the surface 1</p>

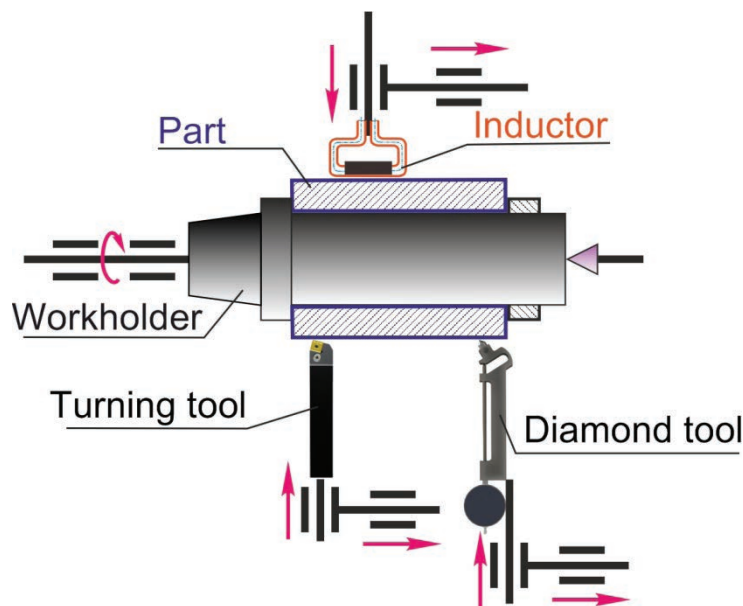


Fig. 10. Integrated part processing scheme

$R_a = 0.4$ microns is assumed through the use of the diamond smoothing process. Based on this, the value of $R_z = 0$, therefore, $t_{\min} = 0$, $t_{\max} = t_{\min} + \delta_t = 0 + 0.0201 = 0.0201 \approx 0.02$ mm.

Solving equations (2) with respect to the required size, we obtain

$$A_{T_{\max}} = A_{K_{\max}} + t_{\min} = 1.0 + 0 = 1.0 \text{ mm};$$

$$A_{T_{\min}} = A_{K_{\min}} + t_{\max} = 0.6 + 0.02 = 0.62 \text{ mm}.$$

5. Determine the allowance for finishing according to the equation

$$z_{i \min} = 2(R_z + T)_{i-1} + 2\sum \delta_{ei} = 0.$$

6. In this case, the preprocessing size of the *surface 1*, taking into account the swelling, will be equal to

$$D_{i-1} = D_i + z_{i \min} + \delta_{i-1} - A_{P_{\min}} = 46 + 0 + 0.01 - 0.00496 = 46.00504 \text{ mm}.$$

Thus, the required parameters are: technological quenching depth $A_T = 0.62^{+0.38}$ mm; preprocessing size $D_I = 46_{-0.050}^{-0.025}$ mm; allowance for final processing $z_{\min} = 0$.

According to the proposed processing scheme, the first transition is the preliminary turning of the part in size $D = 46_{-0.050}^{-0.025}$ mm. Due to the fact that the preprocessing is carried out of raw (non-hardened) material, turning is carried out in more “rigid” modes, in relation to the factory technology. In addition, the considered integrated technology allows improving the technology of forming during machining due to additional heating of the workpiece with a concentrated energy source. Heating of the part with high-frequency currents, carried out before the cutting tool, allows to reduce the cutting resistance, making the workpiece more pliable for shaping, thereby achieving an additional effect that allows to intensify the operating parameters during rough turning. At the same time, the subsequent transition of “HFC quenching” due to heating of structural steel for quenching will make it possible to reduce the effect of the dangerous level of the stress-strain state of the surface layer of the workpiece on the final state of the material.

In order to assign rational modes of surface quenching under hybrid processing conditions, the relationship of the numerical values of the integral temperature-time characteristic with the processing modes of the HEH HFC and with the hardening depth was established.

Figure 11 shows the established minimum values of the $S \in (4.3 > S > 2.5)^\circ\text{C} \cdot \text{s}$, which must be implemented in the surface layers during quenching of pre-eutectoid, eutectoid and trans-eutectoid steels using high-energy heating by high-frequency currents, which ensure the production of carbon-homogeneous austenite at different states of the initial structure of the material [28]. It should be noted that these dependencies (Fig. 11) are obtained as a result of cosimulation of temperature fields and structural-phase transformations in the material, and line 2 is the minimum value of the characteristic S for obtaining 50 % of martensite after cooling. However, as the numerical and full-scale experiment has shown, in most cases the maximum values of the characteristic exceed these values. This is due to the uneven distribution of the characteristic S over the depth of the material. Moreover, the smaller the depth of the hardened layer, the closer the values of the characteristic S are to the recommended values, which once again confirms the greater efficiency of the deep heating scheme in relation to the surface [28, 43–45].

The regularity of the change in the value of the characteristic S corresponds to the nature of the change in the values of the maximum temperatures in the depth of the material. The maximum values of this characteristic for HEH HFC are reached at a depth of about 0.2 mm. Based on this, the dependences of the values of the characteristic S , realized at a depth of 0.2 mm, on the value of the resulting hardened layer were established:

$$S_{45}(h) = 0.55 + 3.69 \cdot h - 5.95 \cdot h^2 + 38.62 \cdot h^3 \quad (3)$$

$$S_{U8}(h) = 0.90 + 3.19 \cdot h - 5.14 \cdot h^2 + 0.18 \cdot h^3 \quad (4)$$

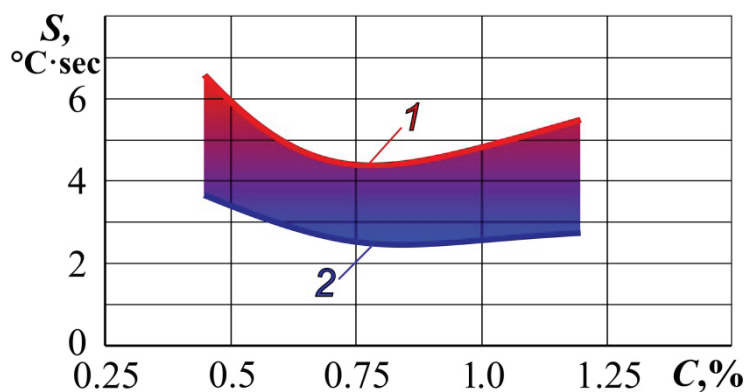


Fig. 11. Dependence of the temperature-time characteristic on the carbon concentration in steel:

1 – obtaining homogeneous austenite; 2 – carbon content in austenite, at which 50% of martensite can be fixed in the cooling stage

To establish the functional dependencies of the integral temperature-time characteristic S on the technological processing modes for the steel grades under consideration, experimental data were processed using the software products *STATISTICA 6.0* and *Table Curve 3D v 4.0*:

$$S(q_s, V_p) = a + bV_p + cq_s + dV_p^2 + eq_s^2 + fV_pq_s + gV_p^3 + hq_s^3 + iV_pq_s^2 + jV_p^2q_s \quad (5)$$

for steel 45:

$$\begin{aligned} a &= -3.601893, \\ b &= 243.31624, \\ c &= 3,048266 \cdot 10^{-7}, \\ d &= -2277.1586, \\ e &= 7.0241349 \cdot 10^{-16}, \\ f &= -8.7904966 \cdot 10^{-6}, \\ g &= -2797.853, \\ h &= 5.5163545 \cdot 10^{-25}, \\ i &= -1.0355329 \cdot 10^{-14}, \\ j &= 6.4796934 \cdot 10^{-5}. \end{aligned}$$

for steel U8A:

$$\begin{aligned} a &= -85.253883, \\ b &= 3173.1572, \\ c &= 4.8366164 \cdot 10^{-7}, \\ d &= -19522.903, \\ e &= 1.8005625 \cdot 10^{-15}, \\ f &= -2.2665061 \cdot 10^{-5}, \\ g &= -122995.64, \\ h &= 4.0624994 \cdot 10^{-24}, \\ i &= -5.344947 \cdot 10^{-14}, \\ j &= 2.7815479 \cdot 10^{-4}. \end{aligned}$$

The maximum error of the measurement does not exceed 5 %.

Since the change in the geometric parameters of the source during the HEH HFC is associated with the labor-intensive manufacture of a new inductor, the specific power of the heating source and the speed of its movement are taken as variable values. Therefore, in the practice of induction heating, it is customary to initially set the size of the source, and then determine the other two technological parameters.

Thus, the simultaneous solution of the system of equations $\begin{cases} S_{45}(h); \\ \frac{S_{45}(q_s, V_p)}{U8} \end{cases}$ will allow to determine the

modes of HEH HFC according to the required quenching depth. However, as the results of mathematical and field experiments have shown, the obtained ranges of hardening modes do not guarantee the formation of a hardened layer without the presence of quenching cracks, the main cause of which is the internal stress state of the material.

Due to the fact that the main technological characteristic of surface hardening is the depth of hardening (the required level of hardness is provided by the selection of the appropriate steel grade), it is possible to influence the magnitude and nature of the distribution of residual stresses only by changing the size of the transition zone.

Taking into account the fact that the seat of destruction of the part in use is the location of the maximum tensile stresses, it is necessary to move the danger zone as far as possible from the surface of the product. Naturally, the depth of occurrence of $\sigma_{t\max}$ will be the greatest if the value of the transition layer turns out to be the maximum. But, in this case, there is a significant decrease in compressive stresses on the surface. The analysis of the results of experimental and theoretical studies has shown that the value of the transition layer should be 25 ... 33 % of the depth of the hardened layer. It is when this requirement is met that there is a certain balance between the fact that the values are shifted to deeper layers of the material and at the same time the value of compressive stresses on the surface decreases on average by no more than 6...10 %. At the same time, large values of the transition zone must be provided when quenching steels with a high carbon content [27, 28, 39, 45].

In this case, when choosing the modes of surface hardening of parts operating under cyclic loads, another criterion is introduced – the relative value of the transition zone $\Psi(q_s, V_p)$, that is, the ratio of the value of the transition zone to the depth of the hardened layer.

As a result of processing the results of experimental studies, the corresponding functional dependencies were obtained for the studied materials and the ranges of processing modes (q_s [W/m²], V_p [m/s]):

$$\Psi(q_s, V_p) = k + lV_p + mq_s + nV_p^2 + oq_s^2 + pV_pq_s + eV_p^3 + sq_s^3 + tV_pq_s^2 + uV_p^2q_s, \quad (6)$$

where $0.25 \leq \Psi(q_s, V_p) \leq 0.33$.

The value of the coefficients of functional dependence:

for steel 45:

$$\begin{aligned} k &= 0.087564, \\ l &= -7.429933, \\ m &= 1.062284 \cdot 10^{-8}, \\ n &= 235.19293, \\ o &= -3.424286 \cdot 10^{-17}, \\ p &= -8.850919 \cdot 10^{-8}, \\ r &= -1309.3045, \\ s &= 2.9423 \cdot 10^{-26}, \\ t &= 1.403793 \cdot 10^{-16}, \\ u &= 1.010925 \cdot 10^{-7}. \end{aligned}$$

for steel U8A:

$$\begin{aligned} k &= 0.013232, \\ l &= 7.354214, \\ m &= 5.814168 \cdot 10^{-9}, \\ n &= 31.678703, \\ o &= -1.724837 \cdot 10^{-17}, \\ p &= -8,746601 \cdot 10^{-8}, \end{aligned}$$

$$r = -543.57972,$$

$$s = 1.233 \cdot 10^{-26},$$

$$t = 1.139227 \cdot 10^{-16},$$

$$u = 2.287546 \cdot 10^{-7}.$$

Thus, the determination of the specific power and the speed of movement of the source during surface

quenching is carried out by solving a system of equations
$$\begin{cases} S_{45/U8}(h); \\ S_{45/U8}(q_s, V_p); \\ \Psi_{45/U8}(q_s, V_p) \end{cases}$$
 for given values of the quench-

ing depth and the relative size of the transition zone. Figure 12 shows a graphical solution to this problem. It can be noted that the obtained range of processing modes is significantly narrower in relation to the purpose of the modes based on providing only a given depth of the hardened layer (curves 1 and 2).

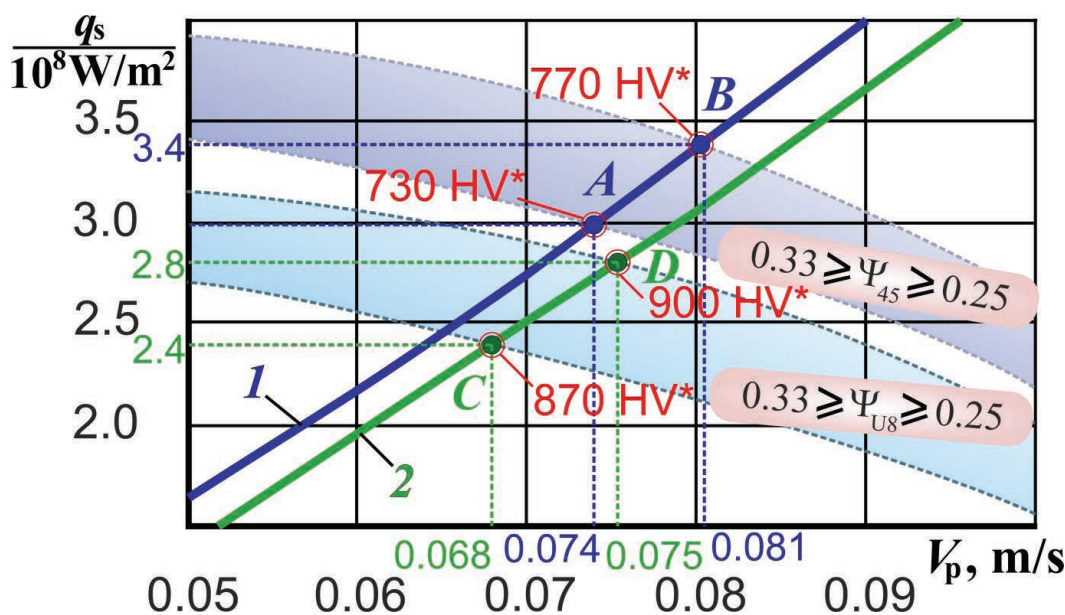


Fig. 12. The dependence of specific power of the source on its speed while hardening steel 45 and U8 by applying HEH HFC to a depth of $h = 0.62$ mm:

1 – steel 45; 2 – steel U8A.

* The level of microhardness of the surface layer of the part, achieved after the transition “Hardening by HFC”

To ensure the depth of the hardened layer $h = 0.62$ mm, we accept the following operating parameters: 1) for steel 45, the range of recommended modes is limited to points A and B on curve 1 – $q_s = (3.0...3.4) \cdot 10^8$ W/m², $V_p = (74...81)$ mm/s;

2) for steel U8A, the range of recommended modes is limited to points C and D on curve 2: in this case, $q_s = (2.4...2.8) \cdot 10^8$ W/m², $V_p = (68...75)$ mm/s.

The obtained processing modes guarantee obtaining the necessary quenching depth and a rational value of the transition zone.

Since hardening is carried out in one setting of the part, then $T_{aux} = 0$ s. In this case, the piece productivity will be equal to the technological productivity.

The calculation of productivity and energy consumption at the transition “HFC hardening” is carried out according to the formulas:

$$P_p = \frac{(V_p/\pi D)b}{L}, \quad E = \frac{q_s b R_s}{P_p} = \frac{q_s b R_s L}{(V_p/\pi D)b}$$

where $L = 104$ mm (Fig. 3), $b = 10$ mm (Fig. 1). The results of calculating energy consumption and productivity during thermal hardening of the part for all combinations of operating parameters and steel grades are presented in Table 4.

Table 4

The results of calculating the productivity and energy consumption of surface hardening by means of HEH HFC under the conditions of integrated processing

Steel, mode	Speed V_p , m/s	Specific power q_s , 10^8 W/m ²	Productivity, s ⁻¹	Energy consumption, kW×h
45	A	0.074	3.0	0.049
	B	0.081	3.4	0.054
U8A	C	0.068	2.4	0.045
	D	0.075	2.8	0.050

The analysis of the obtained results shows that the use of integrated processing allows, in relation to the existing technology at the factory, to increase the productivity of surface hardening using HFC by 3.5...4.1 times, and to reduce energy consumption by 9.5...11.3 times.

Figures 13-14 show the results of optical microscopy, microhardness and residual stress measurements, as well as the results of mathematical simulation for two modes:

1. Steel U8A – the mode indicated by the point C (P_p increases by 3.5 times, and E decreases by 11.3 times): $q_s = 2.4 \cdot 10^8$ W/m², $V_p = 68$ mm/s;

2. Steel 45 – the mode indicated by the point B (P_p increases by 4.1 times, and E decreases by 9.5 times): $q_s = 3.4 \cdot 10^8$ W/m², $V_p = 81$ mm/s.

Analyzing the graphs of the microhardness distribution of the surface layer, three characteristic zones can be distinguished (Fig. 13 a, d and Fig. 14 a, b):

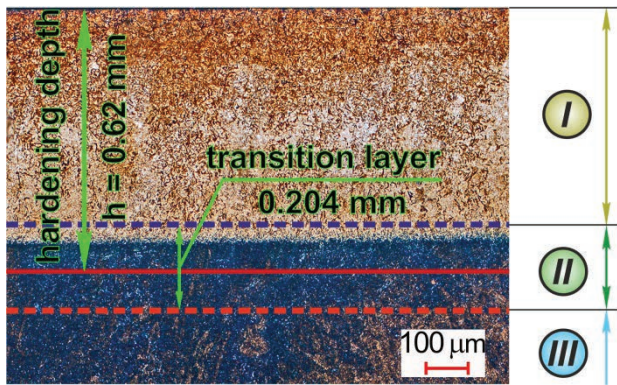
- zone I is characterized by a stable average value of the microhardness level;
- zone II is a transition zone;
- zone III is a zone that has not undergone structural and phase changes.

The depth of the hardened layer is taken as the distance from the surface to the zone with a structure containing 50 % martensite. In turn, the transition layer is the zone between the surface layer of hardened steel with a stable average level of microhardness and the zone of the material in which no structural-phase transformations have occurred.

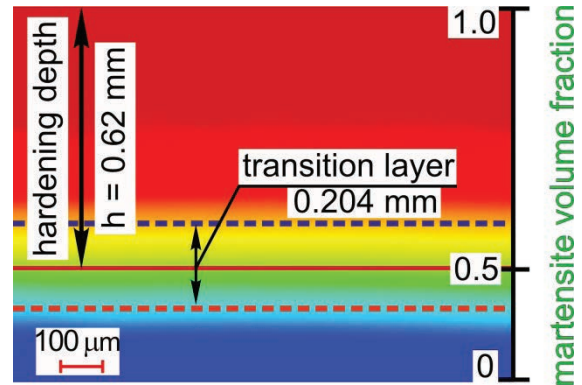
Subsequent diamond smoothing of the surface 1 (Fig. 3) managed to achieve a roughness level of the order of $R_a = 0.1$ μ m (Fig. 15, a), while increasing the microhardness and the level of compressive stresses in the surface layer to values of 870 HV and $\sigma_c = -650$ $\sigma_c = 20$ MPa, respectively (Fig. 15, b).

Conclusion

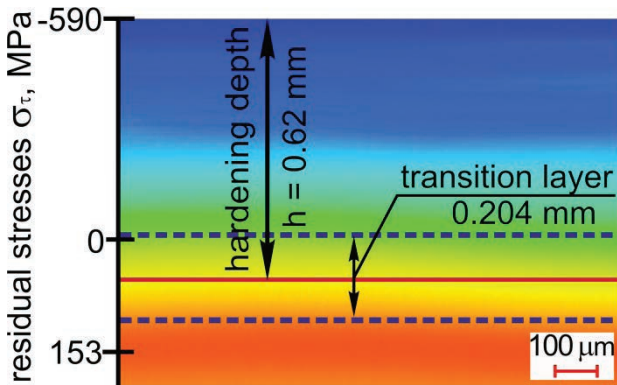
An original method of structural and kinematic analysis for pre-design studies of hybrid metalworking equipment is presented. Methodological recommendations for the modernization of metal-cutting machines have been developed, the implementation of which will make it possible to implement high-energy heating by high frequency currents (HEH HFC) on a standard machine system and ensure the formation of high-tech technological equipment with expanded functionality. A single integral parameter of the temperature-time effect on the structural material is proposed when assigning hardening modes with concentrated heating sources that guarantee the required set of quality indicators of the surface layer of machine parts, while ensuring energy efficiency and processing performance in general. It has been experimentally confirmed that the introduction of the proposed hybrid machine into production in conjunction with the developed recommendations for the appointment of HEH HFC modes in the conditions of integrated processing of a part of the “Plunger barrel” type in relation to the factory technology allows to increase the productivity of



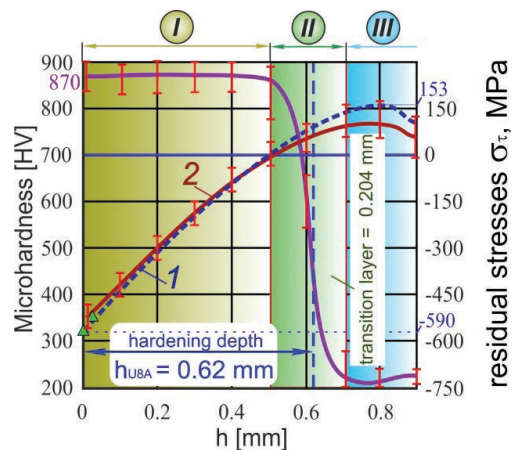
a



b



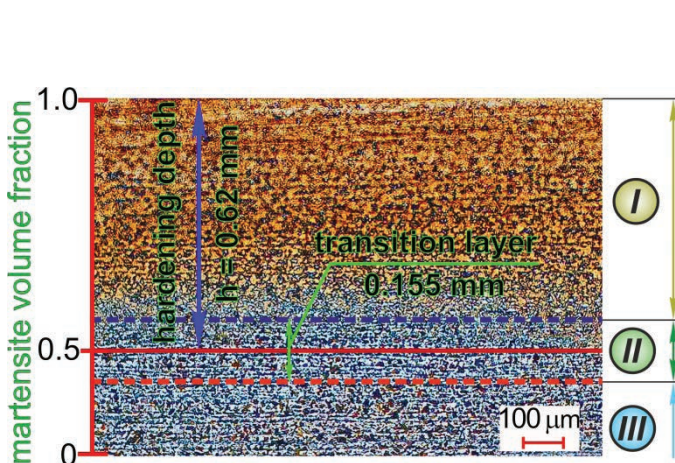
c



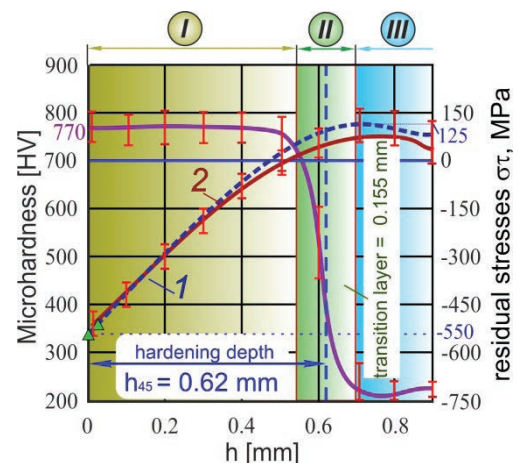
d

Fig. 13. Experimental results for parts made of U8 steel:

a – optical microscopy; b – the simulation results of structural-phase transformations – distribution of the volume fraction of the martensite structure; c – the distribution of tangential residual stresses (simulation results); d – the distribution of microhardness and residual stresses in the surface layer: 1 – a calculated plot of the tangential residual stresses; 2 – a plot of residual stresses obtained experimentally (by mechanical destructive method); ▲ – residual stresses obtained by X-ray determination



a



b

Fig. 14. Experimental results for parts made of 45 steel:

a – optical microscopy; b – the distribution of microhardness and residual stresses in the surface layer: 1 – a calculated plot of the tangential residual stresses; 2 – a plot of residual stresses obtained experimentally (by mechanical destructive method); ▲ – residual stresses obtained by X-ray determination

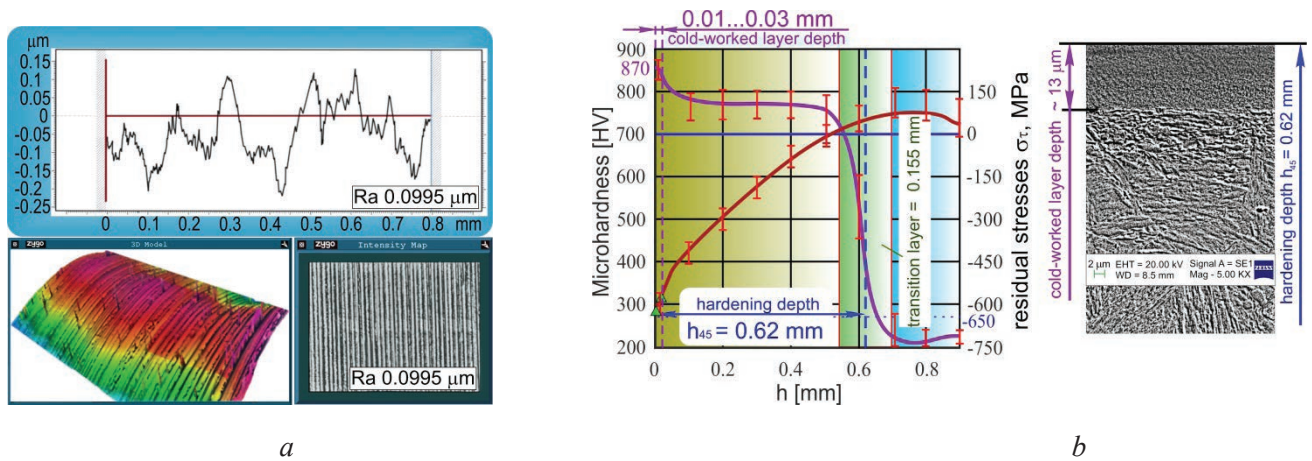


Fig. 15. The quality of the surface layer part after diamond smoothing:

a – topography and surface profilogram; *b* – the distribution of microhardness and residual stresses in the surface layer and its microstructure

surface hardening by 3.5...4.1 times, and reduce energy consumption by 9.5...11.3 times. The implementation of the presented work allowed us to obtain information for solving a critical problem of modern mechanical engineering: ensuring a given high quality of products, reducing the production cycle of manufacturing, minimizing the cost of manufactured products and forming new surface characteristics of parts.

References

1. Brecher C., Özdemir D. *Integrative production technology: theory and applications*. Springer International Publ., 2017. 1100 p. DOI: 10.1007/978-3-319-47452-6. ISBN 978-3-319-47451-9. ISBN 978-3-319-47452-6.
2. Rizzo A., Goel S., Grilli K.M., Iglesias R., Jaworska L., Lapkovskis V., Novak P., Postolnyi B.O., Valerini D. The critical raw materials in cutting tools for machining applications: a review. *Materials*, 2020, vol. 13, p. 1377. DOI: 10.3390/ma13061377.
3. Makarov V.M., Lukina S.V. Unikal'naya sinergiya gibridnykh stankov [Unique synergy of hybrid machines]. *Ritm: Remont. Innovatsii. Tekhnologii. Modernizatsiya = RITM: Repair. Innovation. Technologies. Modernization*, 2016, no. 8, pp. 18–25.
4. Makris S., Aivaliotis P. Framework for accurate simulation and model-based control of hybrid manufacturing processes. *Procedia CIRP*, 2021, vol. 97, pp. 470–475. DOI: 10.1016/j.procir.2020.07.007.
5. Garro O., Martin P., Veron M. Shiva a multiarms machine tool. *CIRP Annals – Manufacturing Technology*, 1993, vol. 42, iss. 1, pp. 433–436. DOI: 10.1016/S0007-8506(07)62479-2.
6. Moriwaki T. Multi-functional machine tool. *CIRP Annals – Manufacturing Technology*, 2008, vol. 57, iss. 2, pp. 736–749. DOI: 10.1016/j.cirp.2008.09.004.
7. Boivie K., Karlsen R., Ystgaard P. The concept of hybrid manufacturing for high performance parts. *South African Journal of Industrial Engineering*, 2012, vol. 23, iss. 2, pp. 106–115.
8. Jeon Y., Lee C.M. Current research trend on laser assisted machining. *International Journal of Precision Engineering and Manufacturing*, 2012, vol. 13, iss. 2, pp. 311–317. DOI: 10.1007/s12541-012-0040-4.
9. Lauwers B., Klocke F., Klink A., Tekkaya A.E., Neugebauer R., McIntosh D. Hybrid processes in manufacturing. *CIRP Annals*, 2014, vol. 63, iss. 2, pp. 561–583. DOI: 10.1016/j.cirp.2014.05.003.
10. Yamazaki T. Development of a hybrid multi-tasking machine tool: integration of additive manufacturing technology with CNC machining. *Procedia CIRP*, 2016, vol. 42, pp. 81–86. DOI: 10.1016/j.procir.2016.02.193.
11. Yanyushkin A.S., Lobanov D.V., Arkhipov P.V. Research of influence of electric conditions of the combined electro-diamond machining on quality of grinding of hard alloys. *IOP Conference Series: Materials Science and Engineering*, 2015, vol. 91, p. 012051. DOI: 10.1088/1757-899X/91/1/012051.
12. Lauwers B., Chernovol N., Peeters B., Camp D.V., Riel T.V., Qian J. Hybrid manufacturing based on the combination of mechanical and electro physical–chemical processes. *Procedia CIRP*, 2020, vol. 95, pp. 649–661. DOI: 10.1016/j.procir.2020.11.003.
13. Berenji K.R., Karagüzel U., Özlü E., Budak E. Effects of turn-milling conditions on chip formation and surface finish. *CIRP Annals*, 2019, vol. 68, iss. 1, pp. 113–116. DOI: 10.1016/j.cirp.2019.04.067.



14. Yang Y., Gong Y., Qu S., Rong Y., Sun Y., Cai M. Densification, surface morphology, microstructure and mechanical properties of 316L fabricated by hybrid manufacturing. *The International Journal of Advanced Manufacturing Technology*, 2018, vol. 97, iss. 5–8, pp. 2687–2696. DOI: 10.1007/s00170-018-2144-1.
15. Guerrini G., Fortunato A., Melkote S.N., Ascari A., Lutey A.H.A. Hybrid laser assisted machining: a new manufacturing technology for ceramic components. *Procedia CIRP*, 2018, vol. 74, pp. 761–764. DOI: 10.1016/j.procir.2018.08.015.
16. Mirzendehtdel A.M., Behandish M., Nelaturi S. Topology optimization with accessibility constraint for multi-axis machining. *Computer-Aided Design*, 2020, vol. 122, p. 102825. DOI: 10.1016/j.cad.2020.102825.
17. Khatir F.A., Sadeghi M.H., Akar S. Investigation of surface integrity in the laser-assisted turning of AISI 4340 hardened steel. *Journal of Manufacturing Processes*, 2021, vol. 61, pp. 173–189. DOI: 10.1016/j.jmapro.2020.09.073.
18. Makarov V.M. Kompleksirovannyye tekhnologicheskyye sistemy: perspektivy i problemy vnedreniya [Well integrated technological systems: prospects and problems of implementation]. *Ritm: Remont. Innovatsii. Tekhnologii. Modernizatsiya = RITM: Repair. Innovation. Technologies. Modernization*, 2011, no. 6 (64), pp. 20–23.
19. Mitsuishi M., Ueda K., Kimura F., eds. *Manufacturing systems and technologies for the new frontier: the 41st CIRP Conference on Manufacturing Systems*, May 26–28, 2008, Tokyo, Japan. London, Springer, 2008. 556 p. ISBN 978-1-84800-267-8. DOI: 10.1007/978-1-84800-267-8.
20. Skeebe V., Pushnin V., Erohin I., Kornev D. Integration of production steps on a single equipment. *Materials and Manufacturing Processes*, 2015, vol. 30, iss. 12, pp. 1408–1411. DOI: 10.1080/10426914.2014.973595.
21. Liu J., Ye C., Dong Y. Recent development of thermally assisted surface hardening techniques: a review. *Advances in Industrial and Manufacturing Engineering*, 2021, vol. 2, p. 100006. DOI: 10.1016/j.aime.2020.100006.
22. Mühl F., Jarms J., Kaiser D., Dietrich S., Schulze V. Tailored bainitic-martensitic microstructures by means of inductive surface hardening for AISI4140. *Materials and Design*, 2020, vol. 195, p. 108964. DOI: 10.1016/j.matdes.2020.108964.
23. Sales W.F., Schoop J., Silva L.R.R., Machado Á.R., Jawahir I.S. A review of surface integrity in machining of hardened steels. *Journal of Manufacturing Processes*, 2020, vol. 58, pp. 136–162. DOI: 10.1016/j.jmapro.2020.07.040.
24. Amigo F.J., Urbikain G., Pereira O., Fernández-Lucio P., Fernández-Valdivielso A., López de Lacalle L.N. Combination of high feed turning with cryogenic cooling on Haynes 263 and Inconel 718 superalloys. *Journal of Manufacturing Processes*, 2020, vol. 58, pp. 208–222. DOI: 10.1016/j.jmapro.2020.08.029.
25. Borisov M.A., Lobanov D.V., Yanyushkin A.S. Gibrinaya tekhnologiya elektrokhimicheskoi obrabotki slozhnoprofil'nykh izdelii [Hybrid technology of electrochemical processing of complex profiles]. *Obrabotka metallov (tekhnologiya, oborudovanie, instrumenty) = Metal Working and Material Science*, 2019, vol. 21, no. 1, pp. 25–34. DOI: 10.17212/1994-6309-2019-21.1-25-34.
26. Gao K., Qin X. Effect of feed path on the spot continual induction hardening for different curved surfaces of AISI 1045 steel. *International Communications in Heat and Mass Transfer*, 2020, vol. 115, p. 104632. DOI: 10.1016/j.icheatmasstransfer.2020.104632.
27. Skeebe V.Yu., Ivantsivsky V.V. *Gibrinoye metalloobratyvyayushchee oborudovanie: povyshenie effektivnosti tekhnologicheskogo protsessa obrabotki detalei pri integratsii poverkhnostnoi zakalki i abrazivnogo shlifovaniya* [Hybrid metal working equipment: improving the effectiveness of the details processing under the integration of surface quenching and abrasive grinding]. Novosibirsk, NSTU Publ., 2018. 312 p. ISBN 978-5-7782-3690-5.
28. Ivantsivsky V.V., Skeebe V.Yu. *Gibrinoye metalloobratyvyayushchee oborudovanie. Tekhnologicheskie aspekty integratsii operatsii poverkhnostnoi zakalki i abrazivnogo shlifovaniya* [Hybrid metal working equipment. Technological aspects of integrating the operations of surface hardening and abrasive grinding]. Novosibirsk, NSTU Publ., 2019. 348 p. ISBN 978-5-7782-3988-3.
29. Ding H.T., Shin Y.C. Laser-assisted machining of hardened steel parts with surface integrity analysis. *International Journal of Machine Tools and Manufacture*, 2010, vol. 50, iss. 1, pp. 106–114. DOI: 10.1016/j.ijmachtools.2009.09.001.
30. You K., Yan G., Luo X., Gilchrist M.D., Fang F. Advances in laser assisted machining of hard and brittle materials. *Journal of Manufacturing Processes*, 2020, vol. 58, pp. 677–692. DOI: 10.1016/j.jmapro.2020.08.034.
31. Karthikeyan K.M.B., Balasubramanian T., Thillaivanan V., Jangetti G.V. Laser transformation hardening of EN24 alloy steel. *Materials Today: Proceedings*, 2020, vol. 22, pt. 4, pp. 3048–3055. DOI: 10.1016/j.matpr.2020.03.440.
32. Li F., Li X., Wang T., Rong Y.(K.), Liang S.Y. In-process residual stresses regulation during grinding through induction heating with magnetic flux concentrator. *International Journal of Mechanical Sciences*, 2020, vol. 172, p. 105393. DOI: 10.1016/j.ijmecsci.2019.105393.



33. Asadzadeh M.Z., Raninger P., Prevedel P., Ecker W., Mücke M. Hybrid modeling of induction hardening processes. *Applications in Engineering Science*, 2021, vol. 5, p. 100030. DOI: 10.1016/j.apples.2020.100030.
34. Areitioaurtena M., Segurajauregi U., Urresti I., Fisk M., Ukar E. Predicting the induction hardened case in 42CrMo4 cylinder. *Procedia CIRP*, 2020, vol. 87, pp. 545–550. DOI: 10.1016/j.procir.2020.02.034.
35. Javaheri V., Haiko O., Sadeghpour S., Valtonen K., Kömi J., Porter D. On the role of grain size on slurry erosion behavior of a novel medium-carbon, low-alloy pipeline steel after induction hardening. *Wear*, 2021, vol. 476, p. 203678. DOI: 10.1016/j.wear.2021.203678.
36. Hammouma C., Zeroug H. Enhanced frequency adaptation approaches for series resonant inverter control under workpiece permeability effect for induction hardening applications. *Engineering Science and Technology, an International Journal*, 2021. DOI: 10.1016/j.jestch.2021.05.010.
37. Skeebeba V.Yu. Gibridnoe tekhnologicheskoe oborudovanie: povyshenie effektivnosti rannikh stadii proektirovaniya kompleksirovannykh metalloobrabatyvayushchikh stankov [Hybrid process equipment: improving the efficiency of the integrated metalworking machines initial designing]. *Obrabotka metallov (tekhnologiya, oborudovanie, instrumenty) = Metal Working and Material Science*, 2019, vol. 21, no. 2, pp. 62–83. DOI: 10.17212/1994-6309-2019-21.2-62-83.
38. Mühl F., Damon J., Dietrich S., Schulze V. Simulation of induction hardening: simulative sensitivity analysis with respect to material parameters and the surface layer state. *Computational Materials Science*, 2020, vol. 184, p. 109916. DOI: 10.1016/j.commatsci.2020.109916.
39. Skeebeba V.Yu., Pushnin V.N., Erokhin I.A., Kornev D.Yu. Analiz napryazhenno-deformirovannogo sostoyaniya materiala pri vysokoenergeticheskom nagreve tokami vysokoi chastoty [Analysis of the stress-strain state of the material under high-energy heating by high frequency currents]. *Obrabotka metallov (tekhnologiya, oborudovanie, instrumenty) = Metal Working and Material Science*, 2014, no. 3 (64), pp. 90–102.
40. Zhong H., Wang Z., Gan J., Wang X., Yang Y., He J., Wei T.T., Qin X. Numerical simulation of martensitic transformation plasticity of 42CrMo steel based on spot continual induction hardening model. *Surface and Coatings Technology*, 2020, vol. 385, p. 125428. DOI: 10.1016/j.surfcoat.2020.125428.
41. Golovin G.F., Zimin N.V. *Tekhnologiya termicheskoi obrabotki metallov s primeneniem induktsionnogo nagreva* [Heat treatment technology of metals using induction heating]. Leningrad, Mashinostroenie Publ., 1990. 87 p. ISBN 5-217-00926-8.
42. Shepelyakovskii K.Z. *Uprochnenie detalei mashin poverkhnostnoi zakalkoi pri induktsionnom nagreve* [Hardening of machine parts by surface hardening during induction heating]. Moscow, Mashinostroenie Publ., 1972. 288 p.
43. Skeebeba V.Y., Ivancivsky V.V., Martyushev N.V. Peculiarities of high-energy induction heating during surface hardening in hybrid processing conditions. *Metals*, 2021, vol. 11, iss. 9, p. 1354. DOI: 10.3390/met11091354.
44. Skeebeba V.Yu., Ivancivsky V.V., Martyushev N.V., Lobanov D.V., Vakhrushev N.V., Zhigulev A.K. Numerical simulation of temperature field in steel under action of electron beam heating source. *Key Engineering Materials*, 2016, vol. 712, pp. 105–111. DOI: 10.4028/www.scientific.net/KEM.712.105.
45. Ivancivsky V.V., Skeebeba V.Yu., Bataev I.A., Lobanov D.V., Martyushev N.V., Sakha O.V., Khlebova I.V. The features of steel surface hardening with high energy heating by high frequency currents and shower cooling. *IOP Conference Series: Materials Science and Engineering*, 2016, vol. 156, p. 012025. DOI: 10.1088/1757-899X/156/1/012025.
46. Fedotenok A.A. *Kinematicheskaya struktura metallovezhushchikh stankov* [Kinematic structure of machine tools]. Moscow, Mashinostroenie Publ., 1970. 408 p.
47. Ptitsyn S.V., Levitskii L.V. *Strukturnyi analiz i sintez kinematiki metallovezhushchikh stankov* [Structural analysis and kinematics synthesis of machine tools]. Kiev, UMK Publ., 1989. 70 p.
48. Ivakhnenko A.G. *Povyshenie effektivnosti rannikh stadii proektirovaniya metallovezhushchikh stankov na osnove strukturnogo sinteza formoobrazuyushchikh sistem*. Diss. dokt. tekhn. nauk [Improving the efficiency of the early stages of designing machine tools based on the structural synthesis of shaping systems. Dr. eng. sci. diss.]. Moscow, 1998. 244 p.
49. Ivakhnenko A.G., Kuts V.V., Erenkov O.Y., Ivakhnenko E.O., Oleinik A.V. Effectiveness of structural-parametric synthesis of metal-cutting systems. *Russian Engineering Research*, 2017, vol. 37, no. 10, pp. 901–905. DOI: 10.3103/S1068798X17100112.
50. Nakaminami M., Tokuma T., Moriwaki M., Nakamoto K. Optimal structure design methodology for compound multi-axis machine tools—I – Analysis of requirements and specifications. *International Journal of Automation Technology*, 2007, vol. 1, no. 2, pp. 78–86. DOI: 10.20965/ijat.2007.p0078.



51. Nakaminami M., Tokuma T., Matsumoto K., Sakashita S., Moriwaki T., Nakamoto K. Optimal structure design methodology for compound multi-axis machine tools–II – Investigation of basic structure. *International Journal of Automation Technology*, 2007, vol. 1, no. 2, pp. 87–93. DOI: 10.20965/ijat.2007.p0087.
52. Mekid S., ed. *Introduction to precision machine design and error assessment. Mechanical and Aerospace Engineering Series*. Boca Raton, CRC Press, 2008. 302 p. ISBN 0849378869. ISBN 978-0849378867.
53. Ivakhnenko A.G., Kuts V.V. *Strukturno-parametricheskii sintez tekhnologicheskikh sistem* [Structural-parametric synthesis of technological systems]. Kursk, KurskSTU Publ., 2010. 151 p.
54. Kuts V.V. *Metodologiya predproektnykh issledovaniy spetsializirovannykh metallozhushchikh sistem*. Diss. dokt. tekhn. nauk [Methodology of pre-design studies of specialized metal-cutting systems. Dr. eng. sci. diss.]. Kursk, 2012. 365 p.
55. Vragov Yu.D. *Analiz komponentov metallozhushchikh stankov (Osnovy komponentiki)* [Analysis of the layout of machine tools. The basics of compositing]. Moscow, Mashinostroenie Publ., 1978. 208 p.
56. Ivakhnenko A.G. *Kontseptual'noe proektirovanie metallozhushchikh sistem. Strukturnyi sintez* [Conceptual design of metal-cutting systems. Structural synthesis]. Khabarovsk, KhGTU Publ., 1998. 124 p.
57. Ptitsyn S.V., Skeebe V.Yu., Chesov Yu.S., Merezhko E.V. Nadezhnost' prognoza kachestva tekhnologicheskogo oborudovaniya [Reliability prediction of quality process equipment]. *Obrabotka metallov (tekhnologiya, oborudovanie, instrumenty) = Metal Working and Material Science*, 2013, no. 2 (59), pp. 33–38.
58. Skeebe V.Yu., Ivancivsky V.V. Reliability of quality forecast for hybrid metal-working machinery. *IOP Conference Series: Earth and Environmental Science*, 2018, vol. 194, iss. 2, p. 022037. DOI: 10.1088/1755-1315/194/2/022037.
59. Skeebe V.Yu., Ivancivsky V.V., Lobanov D.V., Zhigulev A.K., Skeebe P.Yu. Integrated processing: quality assurance procedure of the surface layer of machine parts during the manufacturing step “diamond smoothing”. *IOP Conference Series: Materials Science and Engineering*, 2015, vol. 25, p. 012031. DOI: 10.1088/1757-899X/125/1/012031.
60. Balakshin B.S. *Osnovy tekhnologii mashinostroeniya* [Fundamentals of mechanical engineering technology]. Moscow, Mashinostroenie Publ., 1969. 560 p.
61. Ivashchenko I.A. *Tekhnologicheskie razmernye raschety i sposoby ikh avtomatizatsii* [Technological dimensional calculations and methods of their automation]. Moscow, Mashinostroenie Publ., 1975. 222 p.
62. Vander Voort G.F., ed. *ASM Handbook. Vol. 9. Metallography and Microstructures*. Materials Park, Ohio, USA, ASM International, 2004. 1184 p. ISBN 978-0-87170-706-2.
63. Totten G.E., Howes M., Inoue T. *Handbook of residual stress and deformation of steel*. Materials Park, Ohio, USA, ASM International, 2002. 499 p. ISBN 978-0-87170-729-1.
64. Sharpe W.N., ed. *Springer handbook of experimental solid mechanics*. Leipzig, New York, Springer Science and Business Media, 2008. 1098 p. ISBN 978-0-387-26883-5.
65. Golovin G.F., Zamyatnin M.M. *Vysokochastotnaya termicheskaya obrabotka: voprosy metallovedeniya i tekhnologii* [High-frequency heat treatment: questions of metal science and technology]. Leningrad, Mashinostroenie Publ., 1990. 239 p.

Conflicts of Interest

The author declare no conflict of interest.

© 2021 The Authors. Published by Novosibirsk State Technical University. This is an open access article under the CC BY license (<http://creativecommons.org/licenses/by/4.0/>).

